American Mineralogist, Volume 104, pages 1022–1031, 2019

Elasticity of single-crystal low water content hydrous pyrope at high-pressure and high-temperature conditions

Dawei Fan[1,*], Jingui Xu[1], Chang Lu[2], Sergey N. Tkachev[4], Bo Li[1,3], Zhiling Ye[1,3], Shijie Huang[1,3], Vitali B. Prakapenka[4], and Wenge Zhou[1,*]

[1]Key Laboratory of High-Temperature and High-Pressure Study of the Earth's Interior, Institute of Geochemistry, Chinese Academy of Sciences, Guiyang, Guizhou 550081, China
[2]Department of Geological Sciences, Jackson School of Geosciences, The University of Texas at Austin, Austin, Texas 78712, U.S.A.
[3]University of Chinese Academy of Sciences, Beijing 100049, China
[4]Center for Advanced Radiation Sources, University of Chicago, Chicago, Illinois 60437, U.S.A.

Abstract

The elasticity of single-crystal hydrous pyrope with ~900 ppmw H_2O has been derived from sound velocity and density measurements using in situ Brillouin light spectroscopy (BLS) and synchrotron X-ray diffraction (XRD) in the diamond-anvil cell (DAC) up to 18.6 GPa at room temperature and up to 700 K at ambient pressure. These experimental results are used to evaluate the effect of hydration on the single-crystal elasticity of pyrope at high pressure and high temperature (*P*-*T*) conditions to better understand its velocity profiles and anisotropies in the upper mantle. Analysis of the results shows that all of the elastic moduli increase almost linearly with increasing pressure at room temperature, and decrease linearly with increasing temperature at ambient pressure. At ambient conditions, the aggregate adiabatic bulk and shear moduli (K_{S0}, G_0) are 168.6(4) and 92.0(3) GPa, respectively. Compared to anhydrous pyrope, the presence of ~900 ppmw H_2O in pyrope does not significantly affect its K_{S0} and G_0 within their uncertainties. Using the third-order Eulerian finite-strain equation to model the elasticity data, the pressure derivatives of the bulk [$(\partial K_S/\partial P)_T$] and shear moduli [$(\partial G/\partial P)_T$] at 300 K are derived as 4.6(1) and 1.3(1), respectively. Compared to previous BLS results of anhydrous pyrope, an addition of ~900 ppmw H_2O in pyrope slightly increases the $(\partial K_S/\partial P)_T$, but has a negligible effect on the $(\partial G/\partial P)_T$ within their uncertainties. The temperature derivatives of the bulk and shear moduli at ambient pressure are $(\partial K_S/\partial T)_P = -0.015(1)$ GPa/K and $(\partial G/\partial T)_P = -0.008(1)$ GPa/K, which are similar to those of anhydrous pyrope in previous BLS studies within their uncertainties. Meanwhile, our results also indicate that hydrous pyrope remains almost elastically isotropic at relevant high *P*-*T* conditions, and may have no significant contribution to seismic anisotropy in the upper mantle. In addition, we evaluated the seismic velocities (v_P and v_S) and the v_P/v_S ratio of hydrous pyrope along the upper mantle geotherm and a cold subducted slabs geotherm. It displays that hydrogen also has no significant effect on the seismic velocities and the v_P/v_S ratio of pyrope at the upper mantle conditions.

Keywords: Hydrous pyrope, single-crystal elasticity, high pressure and high temperature, Brillouin light scattering, upper mantle

Introduction

Silicate garnet is an important constituent in the Earth's upper mantle and transition zone (e.g., Anderson and Bass 1984; Anderson 1989; Duffy and Anderson 1989; Ita and Stixrude 1992; McDonough and Sun 1995; Frost 2008; Fan et al. 2009, 2011, 2013, 2015b, 2015c, 2017a; Bina 2013). Mantle compositional models such as pyrolite and piclogite contain ~15 and ~22% of garnet in the upper mantle, respectively (e.g., Ringwood 1975; Bass and Anderson 1984). The percentage can increase to ~40% or even more in the transition zone because pyroxenes progressively dissolve into garnet with increasing pressure (Li B.W. et al. 2018), forming majorite-garnet solid solutions (Herzberg and Gasparik 1991; Ringwood 1991). Garnet is also one of the important minerals for eclogite (e.g., Kimura et al. 2013; Liu 1980; Xu et al. 2019), formed by high-pressure metamorphism of basalt or gabbro at subduction zones (Poli and Schmidt 2002; Ringwood 1982). Although most natural garnets are complex solid solutions, the most significant component of mantle garnets is its Mg end-member pyrope ($Mg_3Al_2Si_3O_{12}$) (Rickwood et al. 1968; Sinogeikin and Bass 2002). Therefore, pyrope or pyrope-rich garnet is an important mantle mineral, irrespective of what compositional model of Earth's mantle is assumed (Ringwood 1975; Ita and Stixrude 1992).

In addition, previous studies have revealed that hydrogen could be incorporated into nominally anhydrous minerals (NAMs) as structurally bound hydroxyl defects (e.g., Ingrin and Skogby 2000; Skogby 2006; Smyth 1987). NAMs in the Earth's mantle thus have significant implications for the Earth's deep water cycle (e.g., Bolfan-Casanova et al. 2000; Hirschmann and Kohlstedt 2012; Hirschmann 2006; Smyth and Jacobsen 2006).

* E-mail: fandawei@vip.gyig.ac.cn (Orcid 0000-0001-7840-2075) and zhouwenge@vip.gyig.ac.cn

0003-004X/19/0007–1022$05.00/DOI: https://doi.org/10.2138/am-2019-6897

Water can incorporate in garnets as OH-defects associated with charge balancing or oxidation-reduction reactions, or it may substitute Si in the hydrogarnet substitution (Lu and Keppler 1997; Withers et al. 1998; Mookherjee and Karato 2010). Pyrope is a well-known hydrous-bearing NAMs phase in the upper mantle (e.g., Ackermann et al. 1983; Rossman et al. 1989). Natural pyrope-rich garnets from ultrahigh-pressure metamorphic rocks and kimberlite xenoliths generally contain tens to hundreds of ppmw H_2O (e.g., Aines and Rossman 1984a, 1984b; Bell and Rossman 1992a, 1992b; Beran and Libowitzky 2006; Li H Y et al. 2018). Moreover, experiments on water solubility in garnets also indicated that pyrope and pyrope-rich garnets could dissolve certain amounts of hydrogen, ranging from a few hundred to ~1000 ppmw H_2O (Geiger et al. 1991; Lu and Keppler 1997; Withers et al. 1998; Mookherjee and Karato 2010).

The accurate knowledge about the elastic property of pyrope or pyrope-rich garnet is critical for deducing seismic velocities and density profiles and further constructing reliable mantle mineralogy models (e.g., Bass and Anderson 1984; Duffy and Anderson 1989; Weidner and Wang 2000; Bass et al. 2008). Up to now, numerous equation of state studies of pyrope using XRD technique at high pressure and high temperature have been reported (e.g., Levien et al. 1979; Sato et al. 1978; Leger et al. 1990; Wang et al. 1998; Zhang et al. 1998; Zou et al. 2012a). Additionally, the elastic properties of pyrope at ambient and high pressure/temperature conditions have also been investigated using theoretical calculations (e.g., Li et al. 2011; Hu et al. 2016). Moreover, the adiabatic bulk and shear moduli of polycrystalline pyrope have been reported up to 24 GPa and 1700 K by ultrasonic interferometry technique (e.g., Sumino and Nishizawa 1978; Suzuki and Anderson 1983; Chen et al. 1997, 1999; Gwanmesia et al. 2006, 2007; Zou et al. 2012b; Chantel et al. 2016). On the other hand, BLS is another common technique to measure the elasticity of minerals (e.g., Speziale et al. 2014; Bass and Zhang 2015). It has tremendous advantages in deriving the complete set of elastic moduli in single-crystal minerals at extremely high *P*-*T* conditions (e.g., Murakami et al. 2007; Fan et al. 2015a; Mao et al. 2015; Yang et al. 2015; Zhang and Bass 2016). There have been several single-crystal elasticity studies on pyrope at ambient conditions (e.g., Leitner et al. 1980; O'Neill et al. 1991), high pressure (e.g., Conrad et al. 1999; Sinogeikin and Bass 2000), and high temperature (e.g., Sinogeikin and Bass 2002) conditions using BLS technique. Recently, Lu et al. (2013) measured the single-crystal elasticity of Fe-bearing pyrope at high *P*-*T* conditions using BLS technique, which provided the detailed description of Fe effect on the elastic moduli of pyrope.

Furthermore, the effect of hydrogen on the elasticity of other major mantle minerals (e.g., olivine, wadsleyite, and ringwoodite) has been studied extensively at ambient-, high-pressure, and high-temperature conditions (e.g., Inoue et al. 1998; Sinogeikin et al. 2003; Wang et al. 2003, 2006; Jacobsen et al. 2004, 2008; Mao et al. 2008, 2010, 2011, 2012). However, there is only one study on the acoustic velocities and single-crystal elastic moduli of hydrous pyrope (~180 ppmw) using BLS technique at ambient conditions (O'Neill et al. 1991). The effect of hydration on the acoustic velocities and elastic moduli of pyrope at high *P*-*T* conditions remains unavailable, even though it is highly desirable to use its single-crystal elasticity for understanding the geodynamic processes of the upper mantle. Up to now, only Fan et al. (2017b) conducted the high *P*-*T* equation of state study of hydrous pyrope using synchrotron-based XRD technique.

In this study, we measured the acoustic velocities (v_P and v_S) of single-crystal hydrous pyrope at high pressures up to ~18.6 GPa and high temperatures up to 700 K using BLS technique and derived its full set of single-crystal elastic moduli at high *P*-*T* conditions. Based on our results, we further evaluated the effects of hydrogen on the elastic moduli, sound velocities, and elastic anisotropies of pyrope. Finally, we applied our results to discuss the hydrogen effect on the velocity profile and v_P/v_S ratio of pyrope in the Earth's upper mantle.

EXPERIMENTAL METHODS

The single-crystal hydrous pyrope was synthesized in a multi-anvil pressure apparatus (YJ-3000T), at the Institute of Geochemistry, Chinese Academy of Sciences, Guiyang, China. More detailed information about the sample synthesis and sample characterization were presented elsewhere by Fan et al. (2017b). Here we briefly report results from electron probe microanalysis (EPMA), Fourier transform infrared (FTIR), and XRD. EPMA results show that our sample is homogeneous with a chemical formula as $Mg_{3.006}Al_{1.995}Si_{3.005}O_{12}$. Hydrogen concentrations were determined by FTIR spectroscopy and the absorption bands were readily attributed to structural bonded hydroxyl groups in pyrope (Geiger et al. 1991; Withers et al. 1998; Mookherjee and Karato 2010). The water content in our sample was determined to be ~900(±100) ppmw using the formula of Bell et al. (1995). Meanwhile, the XRD pattern of our sample confirmed a cubic structure with lattice parameter *a* = 11.460(3) Å at ambient conditions, yielded the unit-cell volume V_0 = 1505.24(8) $Å^3$ and density ρ = 3.557(4) g/cm^3. The unit-cell volume of our hydrous pyrope at ambient conditions is ~0.15% higher than anhydrous pyrope (Zhang et al. 1998; Du et al. 2015), which agrees with previous studies for other mantle minerals (e.g., Smyth et al. 2003; Smyth and Jacobsen 2006; Holl et al. 2008; Ye et al. 2010, 2012).

Pyrope has a cubic structure with only three independent elastic moduli (C_{11}, C_{12}, and C_{44}), and therefore, a single crystallographic orientation is sufficient to constrain all three of them using BLS measurements. The crystallographic plane of sample piece is (0.34, –0.53, 0.92) determined by single-crystal XRD at beamline 13-BMD of the GeoSoilEnviroConsortium for Advanced Radiation Sources (GSECARS) of Advanced Photon Source (APS), Argonne National Laboratory (ANL). We double-side polished our sample pieces to ~20–30 μm thickness with successively finer grits down to a final 3M diamond lapping film of 1 μm grain size. The thinly polished platelet was then cleaved into several square pieces of the desired size (~150 μm) for high-pressure/high-temperature measurements.

High-pressure BLS combined with XRD measurements were conducted on the single-crystal hydrous pyrope in a short symmetrical DAC at 13-BMD beamline of APS. An incident X-ray beam of 0.3344 Å wavelength focused to a 3 × 7 $μm^2$ area was used to determine the unit-cell volume of crystal in the DACs. Round Re gasket of 250 μm thick and 3 mm in diameter was pre-indented to ~55 μm thickness using a pair of 500 μm culet size diamond anvils. Subsequently, a cylindrical 300 μm diameter hole was drilled in the pre-indented area as the sample chamber. A single-crystal platelet with a diameter of ~150 μm was then placed into the sample chamber, together with some ruby spheres of approximately 5 μm in diameter as the pressure indicator (Mao et al. 1986) for neon gas loading as well as for high-pressure experiments. The neon pressure medium was loaded into the sample chamber using the gas-loading system at GSECARS of APS (Rivers et al. 2008). Pressures were measured from ruby fluorescence spectra, while pressure uncertainties were calculated using multiple measurements before and after collection of BLS spectra for each pressure point. The XRD spectra were used to determine density at each pressure before and after BLS measurements (Table 1).

High-temperature BLS experiments were also performed at 13-BMD beamline of APS. A single-crystal hydrous pyrope (~150 μm) was loaded into an externally heated DAC (EHDAC), which was equipped with an alumina ceramic heater coiled with two Pt wires of 200 μm in diameter and 48 cm in length (Kantor et al. 2012; Lu et al. 2013; Yang et al. 2014, 2016; Mao et al. 2015; Fan et al. 2019). Re was used as the gasket material and pre-indented to ~55 μm thickness using a pair of diamond anvils with 500 μm culet size and then a 300 μm diameter sample chamber was drilled at the center of pre-indentation. The single-crystal hydrous pyrope sample was sealed in the sample chamber. An R-type thermocouple was attached to one of diamond surface approximately 500 μm away from its culet and clad with a ceramic adhesive (Resbond

TABLE 1. Densities, elastic moduli, and aggregate velocities of hydrous pyrope at high pressure and ambient temperature

P (GPa)	Density (g/cm^3)	C_{11} (GPa)	C_{12} (GPa)	C_{44} (GPa)	K_V (GPa)	K_R (GPa)	K_S (GPa)	G_V (GPa)	G_R (GPa)	*G* (GPa)	v_P (km/s)	v_S (km/s)	v_P/v_S	*AV*
0.0001	3.557(2)	294.5(5)	105.7(6)	90.5(4)	168.6(4)	168.6(4)	168.6(4)	92.1(2)	92.0(3)	92.0(3)	9.05(1)	5.09(1)	1.78(1)	–0.026(1)
0.9(1)	3.577(2)	301.7(5)	109.9(6)	91.4(4)	173.8(3)	173.8(3)	173.8(3)	93.1(2)	93.2(3)	93.2(3)	9.13(1)	5.10(1)	1.79(1)	–0.030(1)
3.4(2)	3.629(3)	316.8(6)	119.2(7)	94.3(5)	185.1(4)	185.1(4)	185.1(4)	96.0(2)	96.1(2)	96.1(2)	9.29(1)	5.15(1)	1.81(1)	–0.028(1)
5.8(2)	3.677(3)	331.6(6)	126.3(5)	97.7(4)	194.7(5)	194.7(5)	194.7(5)	99.6(2)	99.7(2)	99.7(2)	9.44(1)	5.21(1)	1.81(1)	–0.030(1)
7.5(1)	3.709(2)	339.7(7)	133.5(6)	100.6(5)	202.2(4)	202.2(4)	202.2(4)	101.6(2)	101.6(2)	101.6(2)	9.54(1)	5.23(1)	1.82(1)	–0.015(1)
10.1(2)	3.757(2)	355.2(7)	142.6(7)	103.5(5)	213.5(3)	213.5(3)	213.5(3)	104.6(2)	104.6(3)	104.6(3)	9.69(1)	5.28(1)	1.84(1)	–0.016(1)
12.3(2)	3.795(3)	368.5(8)	150.6(7)	106.8(5)	223.2(3)	223.2(3)	223.2(3)	107.6(1)	107.7(2)	107.7(2)	9.83(1)	5.33(1)	1.85(1)	–0.012(1)
15.5(3)	3.849(3)	387.4(7)	162.5(6)	110.7(6)	237.5(4)	237.5(4)	237.5(4)	111.4(2)	111.4(2)	111.4(2)	10.01(1)	5.38(1)	1.86(1)	–0.009(1)
18.6(2)	3.899(3)	404.6(8)	174.8(8)	115.2(6)	251.4(5)	251.4(5)	251.4(5)	115.1(1)	115.1(2)	115.1(2)	10.19(1)	5.43(1)	1.88(1)	0.0010(2)

Note: Numbers in parentheses represent standard deviations.

TABLE 2. Densities, elastic moduli, and aggregate velocities of hydrous pyrope at ambient pressure and high temperature

T (K)	Density (g/cm^3)	C_{11} (GPa)	C_{12} (GPa)	C_{44} (GPa)	K_V (GPa)	K_R (GPa)	K_S (GPa)	G_V (GPa)	G_R (GPa)	*G* (GPa)	v_P (km/s)	v_S (km/s)	v_P/v_S	*AV*
300[a]	3.557(3)	294.8(6)	105.5(4)	90.7(5)	168.6(5)	168.6(5)	168.6(5)	92.2(3)	92.3(4)	92.3(4)	9.05(1)	5.09(1)	1.78(1)	–0.027(1)
300	3.557(2)	294.5(5)	105.7(6)	90.5(4)	168.6(4)	168.6(4)	168.6(4)	92.0(2)	92.1(3)	92.0(3)	9.05(1)	5.09(1)	1.78(1)	–0.026(1)
400	3.546(3)	291.8(4)	104.9(4)	89.9(2)	167.2(3)	167.2(3)	167.2(3)	91.3(2)	91.3(2)	91.3(2)	9.03(1)	5.07(1)	1.78(1)	–0.024(1)
500	3.534(2)	289.1(5)	104.1(6)	89.3(3)	165.8(3)	165.8(3)	165.8(3)	90.6(1)	90.6(2)	90.6(2)	9.00(1)	5.06(1)	1.78(1)	–0.022(1)
600	3.523(3)	286.6(5)	103.2(5)	88.7(4)	164.3(3)	164.3(3)	164.3(3)	89.9(2)	89.9(2)	89.9(2)	8.98(1)	5.05(1)	1.78(1)	–0.021(1)
700	3.511(3)	283.4(5)	102.3(6)	87.9(4)	162.7(4)	162.7(4)	162.7(4)	89.0(2)	89.0(3)	89.0(3)	8.95(1)	5.03(1)	1.78(1)	–0.019(1)

Note: Numbers in parentheses represent standard deviations.
[a] Represents measurement at temperature decreased from 700 K to room temperature.

920) for temperature measurements. To minimize temperature instability for each heating run, we first heated the sample chamber to a given temperature and then kept it at this temperature for at least 30 min. Temperatures of the sample chamber were actively stabilized within ±1 K using the temperature-power feedback program with a remotely controlled Tektronix Keithley DC power supply during the experiments (Sinogeikin et al. 2006). Single-crystal XRD patterns of hydrous pyrope before and after BLS measurements were also collected to determine the lattice parameters and densities of the sample at high temperatures (Table 2). Temperatures were increased every 100 K from room temperature (300 K) to maximum temperature (700 K), and then decreased to room temperature to check for possible changes in the lattice parameters and elastic moduli at ambient conditions. From Table 2, we can find that the lattice parameters and elastic moduli at ambient conditions of our hydrous pyrope are highly consistent before and after heating. In addition, we did not measure the water content of our sample after the high-temperature BLS measurements due to the relatively small size and thickness of our sample. However, the previous study has determined the water content of the hydrous garnet after heating up to ~1273 K and indicated the water loss of hydrous sample less than 10% (Dai et al. 2012). The maximum experimental temperature in this study (~700 K) is significantly lower than that in previous study (~1273 K) (Dai et al. 2012). Therefore, we infer that there is no obvious water loss during the high temperature BLS measurements in this study, which is also consistent with the previous study that demonstrated that the intrinsic hydrogen loss in hydrous pyrope occurs at temperatures of ≥500 °C (Bell et al. 1995).

The Brillouin system at 13-BMD beamline was equipped with a Coherent Verdi V2 solid-state laser with a wavelength of 532 nm, a Perkin-Elmer photomultiplier detector (model: MP983), and a JRS six-pass tandem Fabry-Pérot interferometer (Lu et al. 2013; Yang et al. 2014). BLS spectra were collected in the symmetric forward scattering geometry with an external scattering angle of 50°, which was calibrated using the elastic moduli of standard silicate glass, distilled water, and single-crystal MgO (Ostwald et al. 1977; Sinogeikin and Bass 2000; Polian et al. 2002). The laser beam focused on the sample position was approximately 15 μm in diameter. The acoustic velocities (v_P and v_S) of our sample were derived from analysis of the measured Brillouin frequency shift as follows:

$$v_{P,S} = \frac{\lambda_0 \Delta v_B}{2\sin\frac{\theta}{2}} \quad (1)$$

where $v_{P,S}$ is the acoustic velocities, λ_0 is the incident laser wavelength, Δv_B is the Brillouin frequency shift, and θ is the external scattering angle.

RESULTS AND DATA ANALYSES

BLS and XRD spectra of single-crystal hydrous pyrope sample are collected up to ~18.6 GPa at room temperature in 2–3 GPa pressure interval and up to 700 K at room pressure in 100 K temperature interval. For all of the Brillouin spectra, one quasi-longitudinal and one quasi-transverse acoustic mode are observed. Typical Brillouin spectra at high-pressure and high-temperature conditions are shown in Figure 1. The measured frequency shifts are converted to velocities along the horizontal axis using Equation 1. Most spectra show strong v_P and v_S peaks with high signal-to-noise ratios except for some crystallographic directions where v_P peaks are weakly observable (Fig. 1). Brillouin signals of neon pressure medium are also observed at pressures below ~8 GPa, but they are too weak to be seen when the pressures are increased above 8 GPa. For each platelet at each given *P*-*T* conditions, Brillouin spectra are collected in 19 different crystallographic directions from 0 to 180° of the azimuthal angle at every 10° (Fig. 2). The variation in measured v_P and v_S as a function of azimuthal angle are not observed outside experimental uncertainties, indicating that our hydrous pyrope is almost elastically isotropic at ambient- and high-pressure and high-temperature conditions (Fig. 2). Furthermore, both v_P and v_S of hydrous pyrope increase with increasing pressure, and decrease with increasing temperature.

Individual elastic moduli (C_{ij}) of single-crystal hydrous pyrope at each given pressure/temperature conditions (Tables 1 and 2) are obtained by fitting the measured spatial dispersion (velocity vs. orientation) of v_P and v_S to Christoffel's equation using nonlinear least square method (Every 1980):

$$\left| C_{ijkl} n_j n_l - \rho v_{P,S}{}^2 \delta_{ik} \right| = 0 \quad (2)$$

where C_{ijkl} is the elastic constant in full suffix notation, n_j and n_l are the direction cosines of the phonon along the propagation direction, ρ is the density at each pressure/temperature condition, δ_{ik} is the Kronecker δ function. The root-mean-square (RMS) deviation of the fitting are about 20 m/s, indicating excellent agreement between measured and calculated sound velocities at ambient- and high-pressure/temperature conditions (Fig. 2). Previous studies also indicated that the single-crystal elastic moduli of pyrope could be calculated by averaging the mea-

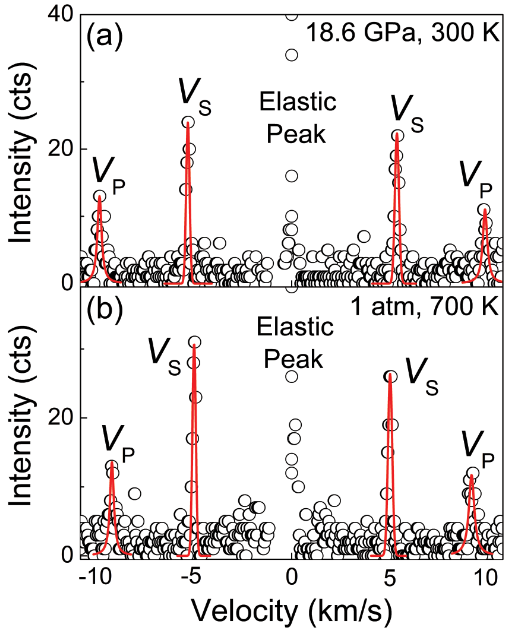

FIGURE 1. Representative Brillouin spectra of single-crystal hydrous pyrope at 18.6 GPa and 300 K (**a**), and 1 atm and 700 K (**b**). Open circles = experimental data; solid lines = fitted v_P and v_S peaks, respectively. The average collection time was ~40 and ~20 min for each spectrum of high-pressure and high-temperature measurements, respectively. The (0.34, –0.53, 0.92) crystallographic plane of single-crystal hydrous pyrope sample was used for both BLS experiments. Experimental uncertainties are smaller than the symbols. (Color online.).

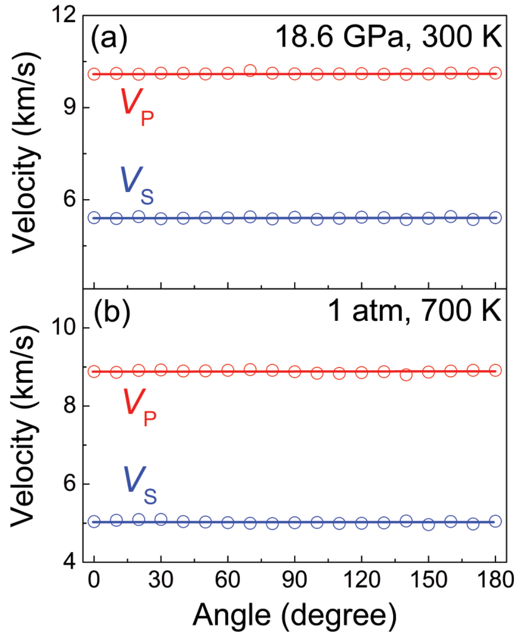

FIGURE 2. v_P and v_S velocities of single-crystal hydrous pyrope as a function of the azimuthal angle measured at 18.6 GPa and 300 K (**a**), and 1 atm and 700 K (**b**). Open circles = experimental data; solid lines = modeled results. Error bars are smaller than the symbols when not shown. (Color online.).

sured acoustic velocities (e.g., Sinogeikin and Bass 2000; Lu et al. 2013). From Supplemental[1] Table S1, we notice that the single-crystal elastic moduli of hydrous pyrope derived from the nonlinear least-squares fitting are indistinguishable within their uncertainties from those calculated values by averaging the measured acoustic velocities assuming that pyrope is elastically isotropic. All of the individual elastic moduli (C_{11}, C_{12}, and C_{44}) for hydrous pyrope increase smoothly with increasing pressure and decrease with increasing temperature (Fig. 3).

Using the derived individual elastic moduli (C_{11}, C_{12}, and C_{44}) of hydrous pyrope, the adiabatic bulk and shear moduli (K_S and G) are calculated according to the Voigt-Reuss-Hill averages (Hill 1952). The aggregate adiabatic bulk (K_{S0}) and shear moduli (G_0) of hydrous pyrope at ambient conditions are 168.6(4) and 92.0(3) GPa, respectively. The pressure derivatives of elastic moduli at 300 K (Tables 3 and 4) are obtained by fitting the elastic moduli at high pressure using the third-order Eulerian finite-strain equation (Figs. 3a and 4a) (Birch 1978). The pressure derivatives of the individual (C_{ij}) and aggregate (K_S and G) elastic moduli at room temperature are derived to be $(\partial C_{11}/\partial P)_T$ = 6.2(1), $(\partial C_{12}/\partial P)_T$ = 3.7(1), $(\partial C_{44}/\partial P)_T$ = 1.5(1), $(\partial K_S/\partial P)_T$ = 4.6(1), and $(\partial G/\partial P)_T$ = 1.3(1), respectively. Due to the limited temperature range for high-temperature data, a linear equation is applied to obtain the temperature derivatives of elastic moduli (Figs. 3b and 4b). The temperature derivative of individual and aggregate elastic moduli at ambient pressure (Tables 3 and 4) are derived to be $(\partial C_{11}/\partial T)_P$ = –0.028(1) GPa/K, $(\partial C_{12}/\partial T)_P$ = –0.009(1) GPa/K, $(\partial C_{44}/\partial T)_P$ = –0.006(1) GPa/K, $(\partial K_S/\partial T)_P$ = –0.015(1) GPa/K, and $(\partial G/\partial T)_P$ = –0.008(1) GPa/K, respectively. The aggregate v_P and v_S of our hydrous pyrope at high-pressure/temperature conditions (Fig. 5) are calculated using the following equations:

TABLE 3. Single-crystal elastic moduli and their pressure and temperature derivatives of hydrous pyrope at ambient conditions in comparison to previous studies [a]

References	Composition	Method	C_{11} (GPa)	C_{12} (GPa)	C_{44} (GPa)	$(\partial C_{11}/\partial P)_T$	$(\partial C_{12}/\partial P)_T$	$(\partial C_{44}/\partial P)_T$	$(\partial C_{11}/\partial T)_P$ (GPa/K)	$(\partial C_{12}/\partial T)_P$ (GPa/K)	$(\partial C_{44}/\partial T)_P$ (GPa/K)
This study	Hydrous Prp_{100}[c]	BLS	294.5(5)	105.7(6)	90.5(4)	6.2(1)	3.7(1)	1.5(1)	–0.028(1)	–0.009(1)	–0.006(1)
O'Neill et al. (1991)	Hydrous Prp_{100}[d]	BLS	296.2(5)	111.1(6)	91.6(3)	–[b]	–[b]	–[b]	–[b]	–[b]	–[b]
Leitner et al. (1980)	Prp_{100}	BLS	295(2)	117(1)	90(3)	–[b]	–[b]	–[b]	–[b]	–[b]	–[b]
Sinogeikin and Bass (2000)	Prp_{100}	BLS	297(3)	108(2)	93(2)	5.8(4)	3.2(4)	1.3(3)	–[b]	–[b]	–[b]
Sinogeikin and Bass (2002)	Prp_{100}	BLS	298(3)	107(2)	93(2)	–[b]	–[b]	–[b]	–0.031(3)	–0.006(2)	–0.007(2)
Lu et al. (2013)	$Prp_{68}Alm_{24}Grs_5$	BLS	290(2)	106(2)	92.2(6)	6.0(1)	3.5(1)	1.2(1)	–0.021(4)	–0.0163(5)	–0.003(1)

Notes: Numbers in parenthesis represent standard deviations. Prp = pyrope; Alm = almandine; Grs= grossular; BLS = Brillouin light scattering.
[a] Only Brillouin scattering results are listed for pyrope garnet.
[b] The value is not available in the text.
[c] ~900 ppmw H_2O.
[d] ~180 ppmw H_2O.

Table 4. Bulk and shear moduli and their pressure and temperature derivatives of hydrous pyrope at ambient conditions in comparison to previous studies[a]

References	Composition	Methods	K_{S0} (GPa)	G_0 (GPa)	$(\partial K_S/\partial P)_T$	$(\partial G/\partial P)_T$	$(\partial K_S/\partial T)_P$ (GPa/K)	$(\partial G/\partial T)_P$ (GPa/K)
This study	Hydrous Prp_{100}	BLS	168.6(4)	92.0(3)	4.6(1)	1.3(1)	−0.015(1)	−0.008(1)
O'Neill et al. (1991)	Hydrous Prp_{100}	BLS	172.8(3)	92.0(2)	–[b]	–[b]	–[b]	–[b]
Leitner et al. (1980)	Prp_{100}	BLS	177(1)	89(1)	–[b]	–[b]	–[b]	–[b]
Conrad et al. (1999)	Prp_{100}	BLS	172.7[c]	92[c]	3.2[c]	1.4[c]	–[b]	–[b]
Sinogeikin and Bass (2000)	Prp_{100}	BLS	171(2)	94(2)	4.1(3)	1.3(2)	–[b]	–[b]
Sinogeikin and Bass (2002)	Prp_{100}	BLS	171(2)	94(2)	–[b]	–[b]	−0.014(2)	−0.009(1)
Lu et al. (2013)	$Prp_{68}Alm_{24}Grs_5$	BLS	168(2)	92(1)	4.4(1)	1.2(1)	−0.017(1)	−0.005(1)
Chen et al. (1999)	Prp_{100}	UI	171(20)	92(1)	5.3(4)	1.6(2)	–[b]	–[b]
Gwanmesia et al. (2006)	Prp_{100}	UI	175(2)	91(1)	3.9(3)	1.7(2)	−0.018(2)	−0.010(1)
Zou et al. (2012)	Prp_{100}	UI	170.0(2)	93.2(1)	4.51(2)	1.51(2)	−0.0170(1)	−0.0107(1)
Chantel et al. (2016)	Prp_{100}	UI	172(2)	89.1(5)	4.38(8)	1.66(5)	−0.018(2)	−0.008(1)

Note: Numbers in parentheses represent standard deviations.
[a] Only Brillouin scattering and ultrasonic interferometry results are listed for pyrope garnet.
[b] The value is not available in the text.
[c] The uncertainty is not available in the text.

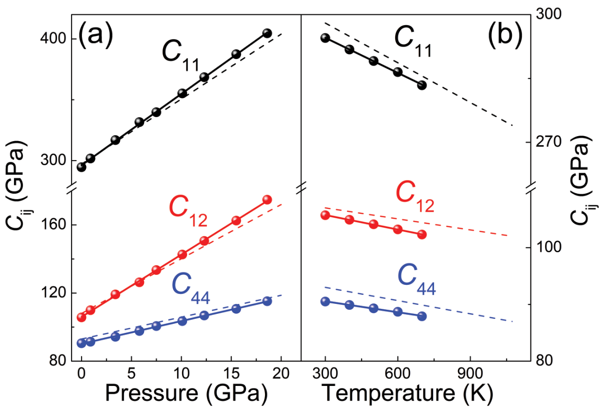

Figure 3. Single-crystal individual elastic moduli (C_{11}, C_{12}, and C_{44}) of hydrous pyrope as a function of pressure (**a**) and temperature (**b**) compared with the previous study of anhydrous pyrope. Solid symbols represent our experimental data; solid lines are modeled results using the third-order finite-strain equation fitting (**a**) or a linear fitting (**b**); dashed lines represent the experimental data of anhydrous pyrope (Sinogeikin and Bass 2000, 2002). Error bars are smaller than the symbols when not shown. (Color online.).

$$v_P = \sqrt{\frac{K_S + \frac{4G}{3}}{\rho}} \quad (3)$$

$$v_S = \sqrt{\frac{G}{\rho}} \quad (4)$$

Discussion

Hydrogen effect on the elasticity of pyrope at high *P-T* conditions

To understand the effect of hydrogen on the elasticity of pyrope, we compare our results with literature values for pyrope obtained from BLS and ultrasonic interferometer measurements. Tables 3 and 4 show a complete list of individual (C_{ij} values) and aggregate (K_{S0} and G_0) elastic moduli obtained in the present study for hydrous pyrope along with those previous studies of anhydrous pyrope. Compared to anhydrous pyrope (e.g., Sinogeikin and Bass 2000, 2002) (Table 3), the addition of ~900 ppmw H_2O in our pyrope sample has negligible effects

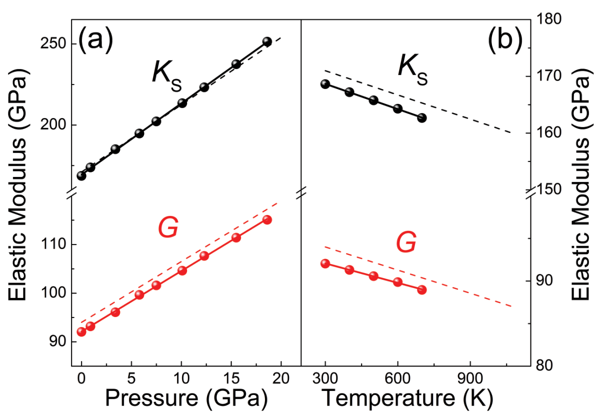

Figure 4. Adiabatic bulk (K_S) and shear modulus (G) of hydrous pyrope as a function of pressure (**a**) and temperature (**b**) compared with the previous study of anhydrous pyrope. Solid symbols represent our experimental data; solid lines are modeled results using the third-order finite-strain equation fitting (**a**) or a linear fitting (**b**); dashed lines represent the experimental data of anhydrous pyrope (Sinogeikin and Bass 2000, 2002). Error bars are smaller than the symbols when not shown. (Color online.).

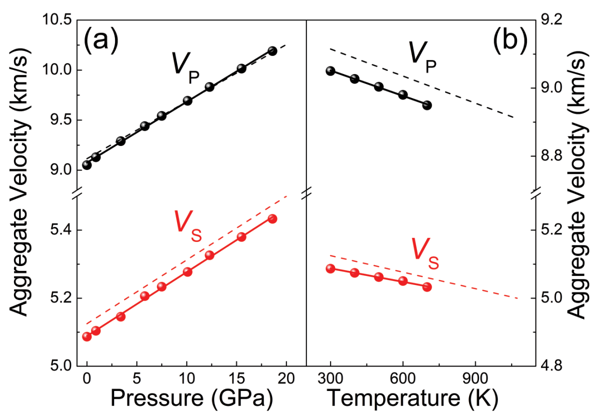

Figure 5. Aggregate compressional (v_P) and shear velocity (v_S) of hydrous pyrope as a function of pressure (**a**) and temperature (**b**) compared with the previous study of anhydrous pyrope. Solid symbols represent our experimental data; solid lines are modeled results using the third-order finite-strain equation fitting (**a**) or a linear fitting (**b**); dashed lines represent the experimental data of anhydrous pyrope (Sinogeikin and Bass 2000, 2002). Error bars are smaller than the symbols when not shown. (Color online.).

on the individual elastic moduli C_{ij} values at ambient conditions within experimental uncertainties. Our aggregate bulk, K_{S0}, and shear moduli, G_0, at ambient conditions of hydrous pyrope are 168.6(4) and 92.0(3) GPa, respectively (Table 4). The presence of ~900 ppmw H_2O in our hydrous pyrope also does not affect the values of K_{S0} and G_0 within experimental uncertainties compared to anhydrous pyrope (Table 4). This is consistent with the conclusion from the study by O'Neill et al. (1991), who deduced that there might have no discernable effect of hydrogen on the elastic properties of pyrope at ambient conditions, though the water solubility in their hydrous pyrope is significantly smaller (~180 ppmw H_2O) than our hydrous pyrope (~900 ppmw H_2O).

Our results also show that hydration has no visible effect on the pressure and temperature derivatives of C_{ij}s in pyrope within experimental uncertainties (Table 3). This is clearly different from the effect of composition (e.g., Fe and Ca) on the temperature derivatives of C_{ij}s in pyrope-rich garnet, where a distinctly larger temperature derivative of C_{12} and lower temperature derivative of C_{11} and C_{44} for (Fe,Ca)-bearing pyrope-rich garnet reported by Lu et al. (2013).

The $(\partial K_S/\partial P)_T$ of our hydrous pyrope is 4.6 (Fig. 4 and Table 4), which is slightly higher than most results of anhydrous pyropes $[(\partial K_S/\partial P)_T = 4.1–4.51]$ (Table 4), except a distinctly lower value $[(\partial K_S/\partial P)_T = 3.2]$ reported by Conrad et al. (1999) and higher value $[(\partial K_S/\partial P)_T = 5.3]$ reported by Chen et al. (1999). Moreover, the $(\partial G/\partial P)_T$ of our hydrous pyrope $[(\partial G/\partial P)_T = 1.3]$ is indistinguishable from most previous studies $[(\partial G/\partial P)_T = 1.3–1.5]$ on anhydrous pyrope within experimental uncertainties, except for two slightly higher values $[(\partial G/\partial P)_T = 1.66$ and $1.7]$ reported from ultrasonic interferometry experiments by Gwanmesia et al. (2006) and Chantel et al. (2016), respectively. Furthermore, our derived $(\partial K_S/\partial T)_P$ and $(\partial G/\partial T)_P$ of hydrous pyrope are indistinguishable from previous BLS values for anhydrous pyrope within their uncertainties, but their absolute values appeared to be slightly lower than most of those from ultrasonic interferometry measurements except a consistent $(\partial G/\partial T)_P$ absolute value reported by Chantel et al. (2016) (Table 4). Therefore, we conclude that the presence of ~900 ppmw H_2O in our pyrope slightly enhances the $(\partial K_S/\partial P)_T$, but does not distinctly affect the K_{S0}, G_0, $(\partial G/\partial P)_T$, $(\partial K_S/\partial T)_P$, and $(\partial G/\partial T)_P$ within their uncertainties.

Hydrogen effect on the elastic anisotropy of pyrope at high *P-T* conditions

Elastic wave anisotropy is a critical feature of the upper mantle (e.g., Karato 1998). One advantage of using single-crystal samples in BLS is that we can obtain the full elastic moduli and put a constraint on the elastic anisotropy. The elastic anisotropy of minerals expresses the difference in stiffness of materials in different crystallographic directions, which can provide insights into seismic anisotropy and can be an indicator of the mechanical stability of materials (e.g., Hu et al. 2016; Sinogeikin and Bass 2000). Thus, knowledge of elastic anisotropy for hydrous pyrope at high *P-T* may shed light on understanding the seismic anisotropy within the Earth's upper mantle.

For the cubic pyrope, the elastic anisotropy factor (A) can be expressed as (Karki et al. 1997; Sinogeikin and Bass 2000):

$$A = \frac{2C_{44} + C_{12}}{C_{11}} - 1 \tag{5}$$

where A indicates the deviation from elastic isotropy, with $A = 0$ for an elastically isotropic material. Analysis of these parameters using our data show that the absolute A values of our hydrous pyrope slightly decreases with increasing pressure and temperature, where A are –0.026 at ambient pressure, 0.001 at 18.53 GPa, and –0.019 at 700 K. Moreover, our hydrous pyrope at ambient conditions has slightly higher absolute A value than anhydrous pyrope (A = –0.006 to –0.008) (e.g., O'Neill et al. 1991; Sinogeikin and Bass 2000, 2002). However, all these absolute A values are still pretty small and very close to zero. Thus, our results indicate that hydrogen does not have a significant effect on the elastic anisotropy of pyrope. Hydrous pyrope remains elastically isotropic at high-pressure and high-temperature conditions compared to the other (olivine, orthopyroxene, and clinopyroxene) major minerals in the upper mantle (e.g., Sang and Bass 2014; Mao et al. 2015; Zhang et al. 2016). Therefore, pyrope may not have a significant contribution to seismic anisotropy in the upper mantle, at least when its water content is less than 900 ppmw.

IMPLICATIONS

Hydrogen effect on the velocity profiles of pyrope in the Earth's upper mantle

The nominally anhydrous minerals (NAMs) in the Earth's deep mantle may serve as a large internal reservoir of water and are important for understanding the evolution and dynamics of Earth's interior (e.g., Bell and Rossman 1992a; Ohtani 2005, 2015; Beran and Libowitzky 2006). Hydration of NAMs has been proposed to correlate with the observed velocity anomalies in the Earth's mantle (e.g., Nolet and Zielhuis 1994; van der Meijde et al. 2003; Song et al. 2004; Ohtani 2005). With the obtained elastic moduli of hydrous pyrope at high *P-T* conditions in this study, we evaluate the effect of hydration on the sound velocities of pyrope at upper mantle conditions.

The presence of ~900 ppmw water in pyrope lowers its v_P and v_S by ~0.7% at ambient conditions (Sinogeikin and Bass 2000). Furthermore, for a better understanding of the hydrogen influence on the velocity behavior of pyrope, we have modeled the velocity profiles of hydrous pyrope along the upper mantle geotherm (Katsura et al. 2010) and a cold subducted slabs geotherm (Eberle et al. 2002) using the updated high-*P*/*T* elasticity results. Our modeling here is limited to the upper-mantle region ranging from 200 to 400 km depth because of the much more complex mineralogical, geochemical, and seismic heterogeneities above 200 km depth (e.g., Jordan 1975; Grand and Helmberger 1984). The modeled results are then compared with the velocity profiles of anhydrous pyrope (Sinogeikin and Bass 2000, 2002) and (Fe, Ca)-bearing pyrope-rich garnet (Lu et al. 2013). Briefly, the third-order Eulerian finite-strain equation and the third-order Birch-Murnaghan equation of state (Birch 1978) are used to obtain the K_S, G, v_P, and v_S of relevant minerals by extrapolating the experimentally derived elastic moduli and their *P-T* derivatives to relevant *P-T* conditions (see Lu et al. 2013 for details). By allowing elastic parameters to vary within

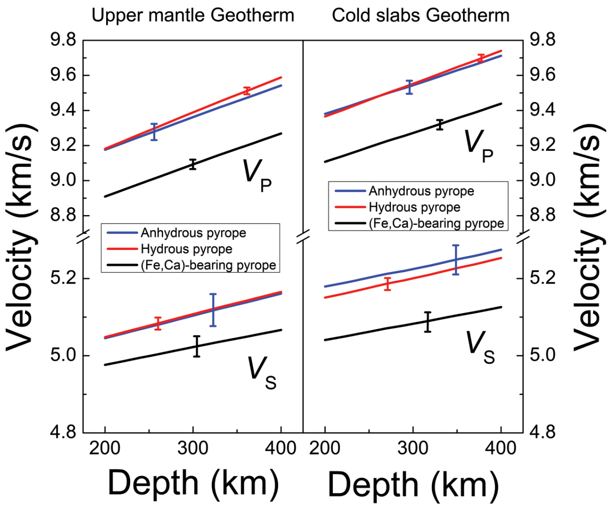

FIGURE 6. Modeled velocities of pyrope garnets in the Earth's upper mantle along the upper mantle geotherm and cold subducted slabs geotherm. Red lines = hydrous pyrope (this study; Fan et al. 2017b); blue lines = anhydrous pyrope (Sinogeikin and Bass 2000, 2002; Zou et al. 2012a); black lines = (Fe,Ca)-bearing pyrope (Lu et al. 2013; Thieblot et al. 1998). Error bars represent the propagated uncertainties (±1σ). (Color online.)

their plausible ranges, the uncertainties (±1σ) of extrapolation results can also be estimated.

Figure 6 shows the calculated velocity-depth relationships of hydrous pyrope along with those of the anhydrous phase. Because of the larger pressure derivative of K_S and similar temperature derivative of K_S, the v_P of hydrous pyrope increases more rapidly with depth than that of anhydrous pyrope. Moreover, the v_P of hydrous pyrope crosses and exceeds that of anhydrous phase at ~200 and ~270 km depth along the upper mantle geotherm and the cold subducted slabs geotherm, respectively. However, considering the error bars presented in Figure 6, the v_P profiles are indistinguishable between hydrous and anhydrous pyrope at 200–400 km depth. Similarly, due to the small effects of hydrogen on the pressure derivative of G, the difference in the v_S between hydrous and anhydrous pyrope is also within the uncertainties over the 200–400 km depth.

On the other hand, hydrogen can enhance the anelasticity (e.g., Karato 1995) and may further change the v_P and v_S. Combining the anelastic effect, the change of v_P and v_S associated with ~900 ppmw H_2O in pyrope at the Earth's upper mantle may be greater than that observed here. However, although up to several hundred ppmw H_2O have been found in some natural garnets (e.g., Aines and Rossman 1984a, 1984b; Li H.Y. et al. 2018), most of the mantle-derived garnets typically contain <100 ppmw H_2O (e.g., Beran and Libowitzky 2006; Ohtani 2015). Combined with the limited effect of ~900 ppmw H_2O on the velocities of pyrope, we thus infer that hydrogen has no significant effect on the velocity profiles of pyrope at upper mantle conditions. Nevertheless, compared to the effect of hydrogen on the velocities of pyrope, the effect of compositions (e.g., Fe and Ca) is significant. Accordingly, the velocity reduction produced by the effect of Fe and Ca is ~2–3% either along the upper mantle geotherm or along the cold subducted slabs geotherm (Fig. 6). Therefore, the elasticity studies of hydrous (Fe, Ca)-bearing pyrope-rich garnet at high *P-T* conditions are needed to provide a more comprehensive understanding of the coupled effect of compositions (e.g., Fe and Ca) and hydration on the elasticity and velocity profiles of garnet and then the Earth's upper mantle.

Hydrogen effect on the v_P/v_S ratio of pyrope in the Earth's upper mantle

The v_P/v_S ratio has been proposed as one of the possible indicators to determine the composition in the deep Earth (e.g., Anderson and Bass 1984; Li and Neuville 2010; Mao et al. 2010; Duan et al. 2018), such as the silica content of continental crust (Christensen 1996). It has been widely used to infer the thermal and compositional state of the upper mantle (e.g., Lee 2003; Niu et al. 2004; Speziale et al. 2005; Afonso et al. 2010). Here, we have investigated the effect of hydration on the v_P/v_S ratio of pyrope. The v_P/v_S ratio of the hydrous pyrope at ambient conditions is 1.78, which is the same as the anhydrous pyrope (1.78) (Sinogeikin and Bass 2000). The v_P/v_S ratio increases with pressure at an average rate of 5.03×10^{-3} GPa^{-1}, but it remains constant with increasing temperature from 300 to 700 K. At the depth of 400 km, the v_P/v_S ratio of the hydrous pyrope increases to 1.86 along the upper mantle geotherm and to 1.85 along the cold subducted slabs geotherm, which are ~0.5% higher than that of the anhydrous phase. A similar increase in the v_P/v_S ratio caused by hydration was observed for ringwoodite (Sinogeikin et al. 2003; Jacobsen and Smyth 2006). However, this contrasts with the behavior of olivine for which a ~0.7% decreased in the v_P/v_S ratio was observed in the hydrous olivine relative to anhydrous phase (Zha et al. 1996; Mao et al. 2010). Figure 7 also shows a comparison of the v_P/v_S ratio for hydrous and anhydrous pyrope with the (Fe,Ca)-bearing pyrope-rich garnet. We notice although all garnets exhibit the increased v_P/v_S ratio with increasing depths, the hydrous pyrope has the highest value throughout the upper

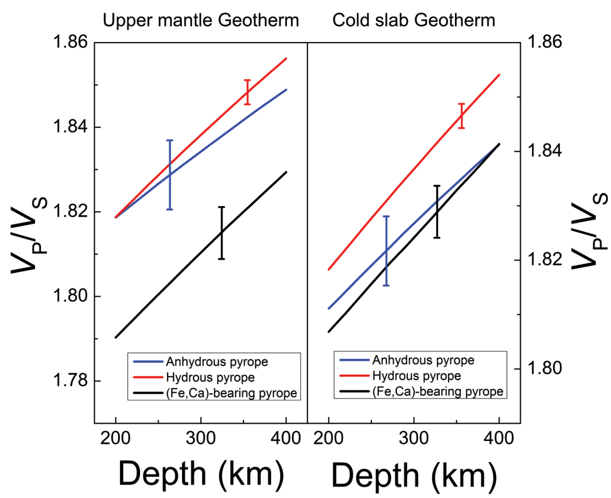

FIGURE 7. Comparison of modeled v_P/v_S ratio of hydrous pyrope with anhydrous pyrope and (Fe,Ca)-bearing pyrope in the Earth's upper mantle along the upper mantle geotherm and cold subducted slabs geotherm. Error bars represent the propagated uncertainties (±1σ). (Color online.)

mantle depths. However, considering the uncertainties of the v_P/v_S ratio presented in Figure 7, the variation of the v_P/v_S ratio among these garnet samples should be limited at 200–400 km depth. This confirms the results of the previous study, which indicated that the variation of mineral composition has only a weak effect on the v_P/v_S ratio of the upper mantle (Duan et al. 2018). Finally, we infer that the hydrogen has also no significant effect on the v_P/v_S ratio of pyrope at upper mantle conditions, especially for the limited hydration level (<100 ppmw H_2O) of mantle-derived garnets.

Funding

D.W. Fan acknowledges financial support from the National Natural Science Foundation of China (41772043), the Joint Research Fund in Huge Scientific Equipment (U1632112) under the cooperative agreement between NSFC and CAS, CAS "Light of West China" Program (Dawei Fan 2017), and Youth Innovation Promotion Association CAS (Dawei Fan 2018434). J.G. Xu acknowledges financial support from the National Natural Science Foundation of China (41802043), and China Postdoctoral Science Foundation (Grant No. 2018M631104). This work was performed at GeoSoilEnviroCARS (The University of Chicago, Sector 13), Advanced Photon Source (APS), Argonne National Laboratory. GeoSoilEnviroCARS is supported by the National Science Foundation (EAR-0622171) and the Department of Energy (DE-FG02-94ER14466) under Contract No. DE-AC02-06CH11357. This research used resources at the Advanced Photon Source, a U.S. Department of Energy (DOE) Office of Science User Facility operated for the DOE Office of Science by Argonne National Laboratory under Contract No. DE-AC02-06CH11357.

Acknowledgments

We thank two anonymous reviewers for their thorough and helpful comments and Jennifer Kung for handling this paper as associate editor. We also thank Z. Mao for providing the Igor fitting code.

References cited

Ackermann, L., Cemič, L., and Langer, K. (1983) Hydrogarnet substitution in pyrope: a possible location for "water" in the mantle. Earth and Planetary Science Letters, 62, 208–214.

Afonso, J.C., Ranalli, G., Fernàndez, M., Griffin, W.L., O'Reilly, S.Y., and Faul, U. (2010) On the V_P/V_S–Mg# correlation in mantle peridotites: Implications for the identification of thermal and compositional anomalies in the upper mantle. Earth and Planetary Science Letters, 289, 606–618.

Aines, R., and Rossman, G.R. (1984a) The hydrous component in garnets: pyralspites. American Mineralogist, 69, 1116–1126.

——— (1984b) Water content of mantle garnets. Geology, 12, 720–723.

Anderson, D.L. (1989) Composition of the Earth. Science, 243, 367–370.

Anderson, D.L., and Bass, J.D. (1984) Mineralogy and composition of the upper mantle. Geophysical Research Letters, 11, 637–640.

Bass, J.D., and Anderson, D.L. (1984) Composition of the upper mantle: geophysical tests of two petrological models. Geophysical Research Letters, 11, 229–232.

Bass, J.D., and Zhang, J.S. (2015) Theory and practice: techniques for measuring high-P–T elasticity. Treatise on Geophysics (second edition), 2, 293–312.

Bass, J.D., Sinogeikin, S.V., and Li, B. (2008) Elastic properties of minerals: A key for understanding the composition and temperature of Earth's interior. Elements, 4, 165–170.

Bell, D.R., and Rossman, G.R. (1992a) Water in Earth's mantle: The role of nominally anhydrous minerals. Science, 255, 1391–1397.

——— (1992b) The distribution of hydroxyl in garnets form the subcontinental mantle of southern Africa. Contributions to Mineralogy and Petrology, 111, 161–178.

Bell, D.R., Ihinger, P.D., and Rossman, G.R. (1995) Quantitative analysis of trace OH in garnet and pyroxenes. American Mineralogist, 80, 465–474.

Beran, A., and Libowitzky, E. (2006) Water in natural mantle minerals II: olivine, garnet and accessory minerals. Reviews in Mineralogy and Geochemistry, 62, 169–191.

Bina, C.R. (2013) Mineralogy: Garnet goes hungry. Nature Geoscience, 6, 335–336.

Birch, F. (1978) Finite strain isotherm and velocities for single-crystal and polycrystalline NaCl at high pressure and 300 K. Journal of Geophysical Research, 83, 1257–1268.

Bolfan-Casanova, N., Keppler, H., and Rubie, D.C. (2000) Water partitioning between nominally anhydrous minerals in the MgO-SiO_2-H_2O system up to 24 GPa: implications for the distribution of water in the Earth's mantle. Earth and Planetary Science Letters, 182, 209–221.

Chantel, J., Manthilake, G.M., Frost, D.J., Beyer, C., Ballaran, T.B., Jing, Z.C., Wang, Y.B. (2016) Elastic wave velocities in polycrystalline $Mg_3Al_2Si_3O_{12}$-pyrope garnet to 24 GPa and 1300 K. American Mineralogist, 101, 991–997.

Chen, G.L., Miletich, R., Mueller, K., and Spetzler, H.A. (1997) Shear and compressional mode measurements with GHz ultrasonic interferometry and velocity-composition systematics for the pyrope-almandine solid solution series. Physics of the Earth and Planetary Interiors, 99, 273–287.

Chen, G.L., Cooke, J.A. Jr., Gwanmesia, G.D., Liebermann, R.C. (1999) Elastic wave velocities of $Mg_3Al_2Si_3O_{12}$-pyrope garnet to 10 GPa. American Mineralogist, 84, 384–388.

Christensen, N.I. (1996) Poisson's ratio and crustal seismology. Journal of Geophysical Research, 101, 3139–3156.

Conrad, P.G., Zha, C.S., Mao, H.K., and Hemley, R.J. (1999) The high-pressure, single-crystal elasticity of pyrope, grossular, and andradite. American Mineralogist, 84, 374–383.

Dai, L.D., Li, H.P., Hu, H.Y., Shan, S.M., Jiang, J.J., and Hui, K.S. (2012) The effect of chemical composition and oxygen fugacity on the electrical conductivity of dry and hydrous garnet at high temperatures and pressures. Contributions to Mineralogy and Petrology, 163, 689–700.

Du, W., Clark, S.M., and Walker, D. (2015) Thermo-compression of pyrope-grossular garnet solid solutions: nonlinear compositional dependence. American Mineralogist, 100, 215–222.

Duan, Y.F., Li, X.Y., Sun, N.Y., Ni, H.W., Tkachev. S.N., and Mao, Z. (2018) Single-crystal elasticity of $MgAl_2O_4$-spinel up to 10.9 GPa and 1000 K: Implication for the velocity structure of the top upper mantle. Earth and Planetary Science Letters, 481, 41–47.

Duffy, T.S., and Anderson, D.L. (1989) Seismic velocities in mantle minerals and the mineralogy of the upper mantle. Journal of Geophysical Research, 94, 1895–1912.

Eberle, M.A., Grasset, O., and Sotin, C. (2002) A numerical study of the interaction between the mantle wedge, subducting slab, and overriding plate. Physics of the Earth and Planetary Interiors, 134, 191–202.

Every, A. (1980) General closed-form expressions for acoustic waves in elastically anisotropic solids. Physical Review B, 22, 1746–1760.

Fan, D.W., Zhou, W.G., Liu, C.Q., Liu, Y.G., Wan, F., Xing, Y.S., Liu, J., Bai, L.G., and Xie, H.S. (2009) The thermal equation of state of $(Fe_{0.86}Mg_{0.07}Mn_{0.07})_3Al_2Si_3O_{12}$ almandine. Mineralogical Magazine, 73, 95–102.

Fan, D.W., Wei, S.Y., Liu, J., Li, Y.C., and Xie, H.S. (2011) High pressure X-ray diffraction study of a grossular-andradite solid solution and the bulk modulus variation along this solid solution. Chinese Physics Letters, 28, 076101.

Fan, D.W., Ma, M.N., Wei, S.Y., Chen, Z.Q., and Xie, H.S. (2013) High pressure elastic behavior of synthetic $Mg_3Y_2(SiO_4)_3$ garnet up to 9GPa. Advances in Materials Science and Engineering, 2013, 502702.

Fan, D.W., Mao, Z., Yang, and Lin, J.F. (2015a) Determination of the full elastic tensor of single crystals using shear wave velocities by Brillouin spectroscopy. American Mineralogist, 100, 2590–2601.

Fan, D.W., Xu, J.G., Ma, M.N., Liu, J., and Xie, H.S. (2015b) *P–V–T* equation of state of spessartine-almandine solid solution measured using a diamond anvil cell and in situ synchrotron X-ray diffraction. Physics and Chemistry of Minerals, 42, 63–72.

Fan, D.W., Xu, J.G., Ma, M.N., Wei, S.Y., Zhang, B., Liu, J., and Xie, H.S. (2015c) *P-V-T* equation of state of $Ca_3Cr_2Si_3O_{12}$ uvarovite garnet by using a diamond-anvil cell and in-situ synchrotron X-ray diffraction. American Mineralogist, 100, 588–597.

Fan, D.W., Kuang, Y.Q., Xu, J.G., Li, B., Zhou, W.G., and Xie, H.S. (2017a) Thermoelastic properties of grossular–andradite solid solution at high pressures and temperatures. Physics and Chemistry of Minerals, 44, 137–147.

Fan, D.W., Lu, C., Xu, J.G., Yan, B.M., Yang, B., and Chen, J.H. (2017b) Effects of water on P-V-T equation of state of pyrope. Physics of the Earth and Planetary Interiors, 267, 9–18.

Fan, D.W., Fu, S.Y., Yang, J., Tkachev, S.N., Prakapenka, V.B., and Lin, J.F. (2019) Elasticity of single-crystal periclase at high pressure and temperature: the effect of iron on the elasticity and seismic parameters of ferropericlase in the lower mantle. American Mineralogist, 104, 262–275.

Frost, D.J. (2008) The upper mantle and transition zone. Elements, 4, 171–176.

Geiger, C.A., Langer, K., Bell, D.R., Rossman, G.R., and Winkler, B. (1991) The hydroxide component in synthetic pyrope. American Mineralogist, 76, 49–59.

Grand, S.P., and Helmberger, D.V. (1984) Upper mantle shear structure of North America. Geophysical Journal International, 76, 399–438.

Gwanmesia, G.D., Zhang, J.Z., Darling, K., Kung, J., Li, B.S., Wang, L.P., Neuville, D., and Liebermann, R.C. (2006) Elasticity of polycrystalline pyrope $(Mg_3Al_2Si_3O_{12})$ to 9 GPa and 1000 °C. Physics of the Earth and Planetary Interiors, 155, 179–190.

Gwanmesia, G.D., Jackson, I., and Liebermann, R.C. (2007) In search of the mixed derivative $\partial^2M/\partial P\partial T$ (M=G, K): joint analysis of ultrasonic data for polycrystalline pyrope from gas- and solid-medium apparatus. Physics and Chemistry of Minerals, 34, 85–93.

Herzberg, C., and Gasparik, T. (1991) Garnet and pyroxenes in the mantle: A test of the majorite fractionation hypothesis. Journal of Geophysical Research,

96, 16263–16274.
Hill, R. (1952) The elastic behaviour of a crystalline aggregate. Proceedings of the Physical Society-Section A, 65, 349–354.
Hirschmann, M. (2006) Water, melting, and the deep earth H_2O cycle. Annual Review of Earth and Planetary Sciences, 34, 629–653.
Hirschmann, M., and Kohlstedt, D. (2012) Water in Earth's mantle. Physics Today, 65, 40–45.
Holl, C.M., Smyth, J.R., Jacobsen, S.D., and Frost, D.J. (2008) Effects of hydration on the structure and compressibility of wadsleyite, β-(Mg_2SiO_4). American Mineralogist, 93, 598–607.
Hu, Y., Wu, Z.Q., Dera, P.K., and Bina, C.R. (2016) Thermodynamic and elastic properties of pyrope at high pressure and high temperature by first-principles calculations. Journal of Geophysical Research, 121, 6462–6476.
Ingrin, J., and Skogby, H. (2000) Hydrogen in nominally anhydrous upper-mantle minerals: concentration levels and implications. European Journal of Mineralogy, 12, 543–570.
Inoue, T., Weidner, D.J., Northrup, P.A., and Parise, J.B. (1998) Elastic properties of hydrous ringwoodite (γ-phase) in Mg_2SiO_4. Earth and Planetary Science Letters, 160, 107–113.
Ita, J., and Stixrude, L. (1992) Petrology, elasticity, and composition of the mantle transition zone. Journal of Geophysical Research, 97, 6849–6866.
Jacobsen, S.D., and Smyth, J.R. (2006) Effect of water on the sound velocities of ringwoodite in the transition zone. In S.D. Jacobsen and S. van der Lee, Eds., Earth's Deep Water Cycle. American Geophysical Union, Washington, D.C., pp. 131–145.
Jacobsen, S.D., Smyth, J.R., Spetzler, H.A., Holl, C.M., and Frost, D.J. (2004) Sound velocities and elastic constants of iron-bearing hydrous ringwoodite. Physics of the Earth and Planetary Interiors, 143-144, 47–56.
Jacobsen, S.D., Jiang, F., Mao, Z., Duffy, T.S., Smyth, J.R., Holl, C.M., and Frost, D.J. (2008) Effects of hydration on the elastic properties of olivine. Geophysical Research Letters, 35, L14303.
Jordan, T.H. (1975) Lateral heterogeneity and mantle dynamics. Nature, 257, 745–750.
Kantor, I., Prakapenka, V., Kantor, A., Dera, P., Kurnosov, A., Sinogeikin, S., Dubrovinskaia, N., and Dubrovinsky, L. (2012) BX90: A new diamond anvil cell design for X-ray diffraction and optical measurements. Review of Scientific Instruments, 83, 125102.
Karato, S. (1995) Effects of water on seismic wave velocities in the upper mantle. Proceedings of the Japan Academy, 71, 61–66.
——— (1998) Seismic anisotropy in the deep mantle, boundary layers and the geometry of mantle convection. Pure and Applied Geophysics, 151, 565–587.
Karki, B.B., Stixrude, L., Clark, S.L., Warren, M.C., Ackland, G.J., and Crain, J. (1997) Structure and elasticity of MgO at high pressure. American Mineralogist, 82, 51–60.
Katsura, T., Yoneda, A., Yamazaki, D., Yoshino, T., Ito, E. (2010) Adiabatic temperature profile in the mantle. Physics of the Earth and Planetary Interiors, 183, 212–218.
Kimura, M., Sugiura, N., Mikouchi, T., Hirajima, T., Hiyagon, H., and Takehana, Y. (2013) Eclogitic clasts with omphacite and pyrope-rich garnet in the NWA 801 CR2 chondrite. American Mineralogist, 98, 387–393.
Lee, C.T.A. (2003) Compositional variation of density and seismic velocities in natural peridotites at STP conditions: implications for seismic imaging of compositional heterogeneites in the upper mantle. Journal of Geophysical Research, 108, B92441.
Leger, J.M., Redon, A.M., and Chateau, C. (1990) Compressions of synthetic pyrope, spessartine and uvarovite garnets up to 25 GPa. Physics and Chemistry of Minerals, 17, 161–167.
Leitner, B.J., Weidner, D.J., and Liebermann, R.C. (1980) Elasticity of single crystal pyrope and implications for garnet solid solution series. Physics of the Earth and Planetary Interiors, 22, 111–121.
Levien, L., Prewitt, C.T., and Weidner, D.J. (1979) Compression of pyrope. American Mineralogist, 64, 805–808.
Li, B.S., and Neuville, D.R. (2010) Elasticity of diopside to 8 GPa and 1073 K and implications for the upper mantle. Physics of the Earth and Planetary Interiors, 183, 398–403.
Li, B.W., Ge, J.H., and Zhang, B.H. (2018) Diffusion in garnet: a review. Acta Geochimica, 37, 19–31.
Li, H.Y., Chen, R.X., Zheng, Y.F., and Hu, Z.C. (2018) Water in garnet pyroxenite from the Sulu orogen: Implications for crust-mantle interaction in continental subduction zone. Chemical Geology, 478, 18–38.
Li, L., Weidner, D.J., Brodholt, J., Alfè, D., and Price, G.D. (2011) Ab initio molecular dynamic simulation on the elasticity of $Mg_3Al_2Si_3O_{12}$ pyrope. Journal of Earth Science, 22, 169–175.
Liu, L.G. (1980) The mineralogy of an eclogitic Earth mantle. Physics of the Earth and Planetary Interiors, 23, 262–267.
Lu, R., and Keppler, H. (1997) Water solubility in pyrope to 100 kbar. Contributions to Mineralogy and Petrology, 129, 35–42.
Lu, C., Mao, Z., Lin, J.F., Zhuravlev, K.K., Tkachev, S.N., and Prakapenka, V.B. (2013) Elasticity of single-crystal iron-bearing pyrope up to 20 GPa and 750 K. Earth and Planetary Science Letters, 361, 134–142.
Mao, H.K., Xu, J., and Bell, P.M. (1986) Calibration of the ruby pressure gauge to 800 kbar under quasi-hydrostatic conditions. Journal of Geophysical Research, 91, 4673–4676.
Mao, Z., Jacobsen, S.D., Jiang, F.M., Smyth, J.R., Holl, C.M., and Duffy, T.S. (2008) Elasticity of hydrous wadsleyite to 12 GPa: implications for Earth's transition zone. Geophysical Research Letters, 35, L21305.
Mao, Z., Jacobsen, S.D., Jiang, F.M., Smyth, J.R., Holl, C.M., Frost, D.J., and Duffy, T.S. (2010) Velocity crossover between hydrous and anhydrous forsterite at high pressures. Earth and Planetary Science Letters, 293, 250–258.
Mao, Z., Jacobsen, S.D., Frost, D.J., McCammon, C.A., Hauri, E.H., and Duffy, T.S. (2011) Effect of hydration on the single-crystal elasticity of Fe-wadsleyite to 12 GPa. American Mineralogist, 96, 1606–1612.
Mao, Z., Lin, J.F., Jacobsen, S.D., Duffy, T.S., Chang, Y.Y., Smyth, J.R., Frost, D.J., Hauri, E.H., and Prakapenka, V.B. (2012) Sound velocities of hydrous ringwoodite to 16 GPa and 673 K. Earth and Planetary Science Letters, 331-332, 112–119.
Mao, Z., Fan, D.W., Lin, J.F., Yang, J., Tkachev, S.N., Zhuravlev, K., and Prakapenka, V.B. (2015) Elasticity of single-crystal olivine at high pressures and temperatures. Earth and Planetary Science Letters, 426, 204–215.
McDonough, W.F., and Sun, S.S. (1995) The composition of the Earth. Chemical Geology, 120, 223–253.
Mookherjee, M., and Karato, S. (2010) Solubility of water in pyrope-rich garnet at high pressures and temperature. Geophysical Research Letters, 37, L03310.
Murakami, M., Sinogeikin, S.V., Hellwig, H., Bass, J.D., and Li, J. (2007) Sound velocity of $MgSiO_3$ perovskite to Mbar pressure. Earth and Planetary Science Letters, 256, 47–54.
Niu, F., Levander, A., Cooper, C.M., Lee, C.T.A., Lenardic, A., and James, D.E. (2004) Seismic constraints on the depth and composition of the mantle keel beneath the Kaapvaal craton. Earth and Planetary Science Letters, 224, 337–346.
Nolet, G., and Zielhuis, A. (1994) Low S velocities under the Tornquist-Teisseyre zone: evidence for water injection into the transition zone by subduction. Geophysical Research Letters, 99, 15813–15820.
Ohtani, E. (2005) Water in the mantle. Elements, 1, 25–30.
——— (2015) Hydrous minerals and the storage of water in the deep mantle. Chemical Geology, 418, 6–15.
O'Neill, B., Bass, J.D., Rossman, G.R., Geiger, C.A., and Langer, K. (1991) Elastic properties of pyrope. Physics and Chemistry of Minerals, 17, 617–621.
Ostwald, J., Pazold, W., and Weis, O. (1977) High-resolution Brillouin spectroscopy of water. Applied Physics, 13, 351–356.
Poli, S., and Schmidt, M.W. (2002) Petrology of subducted slabs. Annual Review of Earth and Planetary Sciences, 30, 207–235.
Polian, A., Vo-Thanh, D., and Richet, P. (2002) Elastic properties of α-SiO_2 up to 2300 K from Brillouin scattering measurements. Europhysics Letters, 57, 375–381.
Rickwood, P.C., Mathias, M., and Siebert, J.C. (1968) A study of garnets from eclogite and peridotite xenoliths found in kimberlite. Contributions to Mineralogy and Petrology, 19, 271–301.
Ringwood, A.E. (1975) Composition and petrology of the Earth's mantle. McGraw-Hill, New York.
——— (1982) Phase transformations and differentiation in subducted lithosphere: implications for mantle dynamics, basalt petrogenesis, and crustal evolution. The Journal of Geology, 90, 611–643.
——— (1991) Phase transformations and their bearing on the constitution and dynamics of the mantle. Geochimica et Cosmochimica Acta, 55, 2083–2110.
Rivers, M., Prakapenka, V.B., Kubo, A., Pullins, C., Holl, C.M., and Jacobsen, S.D. (2008) The COMPRES/GSECARS gas-loading system for diamond anvil cells at the Advanced Photon Source. High Pressure Research, 28, 273–292.
Rossman, G.R., Beran, A., and Langer, K. (1989) The hydrous component of pyrope from the Dora Maira Massif, Western Alps. Physics and Chemistry of Minerals, 1, 151–154.
Sang, L.Q., and Bass, J.D. (2014) Single-crystal elasticity of diopside to 14 GPa by Brillouin scattering. Physics of the Earth and Planetary Interiors, 228, 75–79.
Sato, Y., Akaogi, M., and Akimoto, S. (1978) Hydrostatic compression of the synthetic garnets pyrope and almandine. Journal of Geophysical Research, 83, 335–338.
Sinogeikin, S.V., and Bass, J.D. (2000) Single-crystal elasticity of pyrope and MgO to 20 GPa by Brillouin scattering in the diamond cell. Physics of the Earth and Planetary Interiors, 120, 43–62.
——— (2002) Elasticity of pyrope and majorite-pyrope solid solutions to high temperatures. Earth and Planetary Science Letters, 203, 549–555.
Sinogeikin, S.V., Bass, J.D., and Katsura, T. (2003) Single-crystal elasticity of ringwoodite to high pressures and high temperatures: implications for 520 km seismic discontinuity. Physics of the Earth and Planetary Interiors, 136, 41–66.
Sinogeikin, S.V., Bass, J.D., Prakapenka, V., Lakshtanov, D., Shen, G., Sanchez-Valle, C., and Rivers, M. (2006) Brillouin spectrometer interfaced with synchrotron radiation for simultaneous X-ray density and acoustic velocity measurements. Review of Scientific Instruments, 77, 103905.
Skogby, H. (2006) Water in natural mantle minerals I: Pyroxenes. Reviews in

Mineralogy and Geochemistry, 62, 155–167.
Smyth, J.R. (1987) β-Mg_2SiO_4: A potential host for water in the mantle? American Mineralogist, 72, 1051–1055.
Smyth, J.R., and Jacobsen, S.D. (2006) Nominally anhydrous minerals and Earth's deep water cycle. In S.D. Jacobsen and S. van der Lee, Eds., Earth's Deep Water Cycle. Geophysical Monograph Series, vol. 168, p. 1–11. American Geophysical Union, Washington, D.C.
Smyth, J.R., Holl, C.M., Frost, D.J., Jacobsen, S.D., Langenhorst, F., and McCammon, C.A. (2003) Structural systematics of hydrous ringwoodite and water in Earth's interior. American Mineralogist, 88, 1402–1407.
Song, T.A., Helmberger, D.V., and Grand, S.P. (2004) Low-velocity zone atop the 410-km seismic discontinuity in the northwestern United States. Nature, 427, 530–533.
Speziale, S., Jiang, F., and Duffy, T.S. (2005) Compositional dependence of the elastic wave velocities of mantle minerals: implications for seismic properties of mantle rocks. Geophysical Monograph Series, 160, pp. 301–320. American Geophysical Union, Washington, D.C.
Speziale, S. Marquardt, H., and Duffy, T.S. (2014) Brillouin scattering and its application in geosciences. Reviews in Mineralogy & Geochemistry, 78, 543–603.
Sumino, Y., and Nishizawa, O. (1978) Temperature variation of elastic constants of pyrope-almandine garnets. Journal of Physics of the Earth, 26, 239–252.
Suzuki, I., and Anderson, O.L. (1983) Elasticity and thermal expansion of a natural garnet up to 1000 K. Journal of Physics of the Earth, 31, 125–138.
Thieblot, L., Roux, J., and Richet, P. (1998) High-temperature thermal expansion and decompositions of garnets. European Journal of Mineralogy, 10, 7–15.
van der Meijde, M., Marone, F., Giardini, D., and van der Lee, S. (2003) Seismic evidence for water deep in Earth's upper mantle. Science, 300, 1556–1558.
Wang, J., Sinogeikin, S.V., Inoue, T., and Bass, J.D. (2003) Elastic properties of hydrous ringwoodite. American Mineralogist, 88, 1608–1611.
Wang, J., Sinogeikin, S.V., Inoue, T., and Bass, J.D. (2006) Elastic properties of hydrous ringwoodite at high-pressure conditions. Geophysical Research Letters, 33, L14308.
Wang, Y., Weidner, D.J., Zhang, J., Gwanrnesia, G.D., Liebermann, R.C., and Bass, J.D. (1998) Thermal equation of state of garnets along the pyrope-majorite join. Physics of the Earth and Planetary Interiors, 105, 59–71.
Weidner, D.J., and Wang, Y. (2000) Phase transformations: implications for mantle structure. Geophysical Monograph Series, 117, p. 215–235. American Geophysical Union, Washington, D.C.
Withers, A.C., Wood, B.J., and Carroll, M.R. (1998) The OH content of pyrope at high pressure. Chemical Geology, 147, 161–171.
Xu, J.G., Zhang, D.Z., Fan, D.W., Dera, P., Shi, F., and Zhou, W.G. (2019) Thermoelastic properties of eclogitic ternary garnets and omphacites: Implications for deep subduction of oceanic crust and density anomalies in the upper mantle. Geophysical Research Letters, 46, 179–188.
Yang, J., Mao, Z., Lin, J.F., and Prakapenka, V.B. (2014) Single-crystal elasticity of the deep-mantle magnesite at high pressure and temperature. Earth and Planetary Science Letters, 392, 292–299.
Yang, J., Tong, X.Y., Lin, J.F., Okuchi, T., and Tomioka, N. (2015) Elasticity of ferropericlase across the spin crossover in the Earth's lower mantle. Scientific Reports, 5, 17188.
Yang, J., Lin, J.F., Jacobsen, S.D., Seymour, N.M., Tkachev, S.N., and Prakapenka, V.B. (2016) Elasticity of ferropericlase and seismic heterogeneity in the Earth's lower mantle. Journal of Geophysical Research, 121, 8488–8500.
Ye, Y., Smyth, J.R., Hushur, A., Manghnani, M.H., Lonappan, D., Dera, P., and Frost, D.J. (2010) Crystal structure of hydrous wadsleyite with 2.8% H_2O and compressibility to 60 GPa. American Mineralogist, 95, 1765–1772.
Ye, Y., Brown, D.A., Smyth, J.R., Panero, W.R., Jacobsen, S.D., Chang, Y.Y., Townsend, J.P., Thomas, S.M., Hauri, E.H., Dera, P., and Frost, D.J. (2012) Compressibility and thermal expansion of hydrous ringwoodite with 2.5(3) wt% H_2O. American Mineralogist, 97, 573–582.
Zha, C.S., Duffy, T.S., Downs, R.T., Mao, H.K., and Hemley, R.J. (1996) Sound velocity and elasticity of single-crystal forsterite to 16 GPa. Journal of Geophysical Research, 101, 17535–17545.
Zhang, J.S., and Bass, J.D. (2016) Single-crystal elasticity of natural Fe-bearing orthoenstatite across a high-pressure phase transition. Geophysical Research Letters, 43, 8473–8481.
Zhang, L., Ahsbahs, H., and Kutoglu, A. (1998) Hydrostatic compression and crystal structure of pyrope to 33 GPa. Physics and Chemistry of Minerals, 25, 301–307.
Zou, Y.T., Gréaux, S., Irifune, T., Whitaker, M.L., Shinmei, T., and Higo, Y. (2012a) Thermal equation of state of $Mg_3Al_2Si_3O_{12}$ pyrope garnet up to 19 GPa and 1,700 K. Physics and Chemistry of Minerals, 39, 589–598.
Zou, Y.T., Irifune, T., Gréaux, S., Whitaker, M.L., Shinmei, T., Ohfuji, H., Negishi, R., and Higo, Y. (2012b) Elasticity and sound velocities of polycrystalline $Mg_3Al_2(SiO_4)_3$ garnet up to 20 GPa and 1700 K. Journal of Applied Physics, 112, 014910.

Manuscript received November 14, 2018
Manuscript accepted April 9, 2019
Manuscript handled by Jennifer Kung